Check for updates

OPEN

Dewetting behavior of Ge layers on SiO₂ under annealing

A. A. Shklyaev✉ & A. V. Latyshev

The solid-state dewetting phenomenon in Ge layers on SiO₂ is investigated as a function of layer thickness d_{Ge} (from 10 to 86 nm) and annealing temperature. The dewetting is initiated at about 580–700 °C, depending on d_{Ge}, through the appearance of surface undulation leading to the particle formation and the rupture of Ge layers by narrow channels or rounded holes in the layers with the thicknesses of 10–60 and 86 nm, respectively. The channel widths are significantly narrower than the distance between the particles that causes the formation of thinned Ge layer areas between particles at the middle dewetting stage. The thinned areas are then agglomerated into particles of smaller sizes, leading to the bimodal distributions of the Ge particles which are different in shape and size. The existence of a maximum in the particle pair correlation functions, along with the quadratic dependence of the corresponding particle spacing on d_{Ge}, may indicate the spinodal mechanism of the dewetting in the case of relatively thin Ge layers. Despite the fact that the particle shape, during the solid-state dewetting, is not thermodynamically equilibrium, the use of the Young's equation and contact angles allows us to estimate the particle/substrate interface energy.

The solid-state dewetting phenomenon can be used for the development of the simple and highly productive fabrication methods of dense nano- and micro-sized particle arrays[1–6]. The metal particles obtained by dewetting are widely used due to their ability of surface plasmon generation[7–9]. At the same time, the submicron- and micron-sized dielectric particles, when interacting with light, generate magnetic and electrical resonances. The strong magnetic dipole resonance is excited in particles of materials with a high refractive index (n) under the condition $\lambda \approx nd$, where λ is the incident light wavelength and d is the particle size[10]. In this aspect, Si submicron structures are widely studied. Taking into account that the refractive index of Ge is greater than that of Si and the spectral dependence of their light absorption coefficients, Ge appears as a promising material for electromagnetic resonance engineering in the near infrared spectral range[11–15]. The Ge particle formation can occur by means of the solid-state dewetting phenomenon during annealing of Ge layers on SiO₂. The particles are formed spontaneously and acquire broad distributions in shape and size. The surfaces coated with such particles exhibit strong antireflection properties in a wide spectral range[16]. This initiates the study of light scattering by quasi-random surface structures which can also be formed by other methods[17–20].

Initially, the study of the Ge particle formation on SiO₂ surfaces was aimed at obtaining nanometer-sized three-dimensional Ge islands in the range from several to about 40 nm, which were considered to serve as quantum dots[21–28]. It was shown that Ge islands can be formed at relatively low temperatures, i.e. after annealings at $T \geq 275$ °C of the samples with a Ge layer grown on SiO₂ at room temperature[29], or during the Ge deposition at $T \geq 320$ °C by the molecular-beam technique[23]. The possibility of obtaining pure Ge islands (particles) of larger sizes, according to our knowledge, has not been investigated, whereas the submicron- and micron-sized dielectric particles are required for the photonic application in the visible and infrared spectral ranges. Rather large silicon-rich Ge particles (100–200 nm in the lateral dimension) can be created by means of annealing strained Ge/Si/SiO₂/Si structures at 700 °C[30]. Recently, the large-sized SiGe particles have been grown by the relatively thick Ge layer (~ 40 nm) deposition at 800 °C on Si/SiO₂[16]. When using thick continuous Ge layers on SiO₂ for their subsequent annealing at relatively low temperatures, the dewetting driving force may be insufficient for the layer agglomeration into arrays of individual particles. This effect is known for metal layers on dewetting surfaces, for which it was found that the minimum temperature necessary for the layer agglomeration is higher for thicker metal layers[1,31,32]. The thickness dependence of the dewetting process of Ge layers on SiO₂ is less studied. Cheynis et al. showed that the time for completing the dewetting process increases with the thickness in the 10–40 nm range at a given temperature of about 800 °C[33]. It was also found that the dewetting behavior of 60-nm Ge layers depends on the Ge deposition method[34].

A.V. Rzhanov Institute of Semiconductor Physics, SB RAS, Novosibirsk 630090, Russia. ✉email: shklyaev@isp.nsc.ru
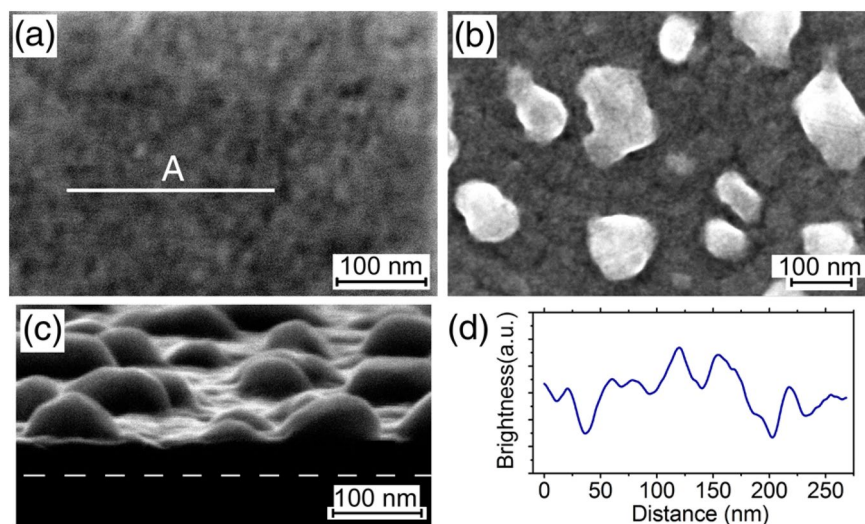
1

Figure 1. (**a**–**c**) SEM images of 20, 86 and 60 nm Ge layers deposited on SiO$_2$ at RT with a subsequent annealing in vacuum for 30 min at 560, 700 and 650 °C, respectively. (**d**) The brightness profile along line A is shown in (**a**). The white dashed line in (**c**) shows the position of the Ge/SiO$_2$ interface, which is not visible due to the increased image contrast. Images (**a,b**) are taken at the normal electron beam incidence and (**c**) at a glancing angle of about 10° relative to the sample surface.

The Ge particle formation on SiO$_2$ can be carried out in two ways. This can occur during the Ge deposition if the substrate temperature is sufficiently high[21,35–37]. Ge particles can also be formed as a result of the high-temperature annealing of continuous Ge layers grown on SiO$_2$ at relatively low temperatures[22,24,29,33,34]. The second approach gives greater opportunities, since it allows avoiding the SiO$_2$ surface etching during the Ge deposition, which occurs via the formation of volatile SiO and GeO molecules[21,38]. The annealing of grown structures can be performed directly in the growth chamber or after the sample removal into the air. In the latter case, the Ge layer surface is covered with a native oxide, which can interfere with the subsequent dewetting process[39] requiring a higher temperature for its initiation than in the first case. However, placing the sample in the air can happen for technological reasons, for example, for carrying out lithography. It is reasonable to assume that the native Ge oxide, similar to the chemically grown Si oxide[39], can affect the minimum temperature for the dewetting process activation.

In this study, in order to obtain submicron-sized Ge particles, we use rather thick (from 10 to 86 nm) continuous Ge layers initially deposited on SiO$_2$ at room temperature (RT) for a subsequent high-temperature annealing. As expected, the layers are thermally unstable and agglomerated into compact particles at 600 °C and higher temperatures depending on their thickness (d_{Ge}). Their agglomeration into particles occurs through the solid-state dewetting. The features of the process indicate that at d_{Ge} of 10–40 nm, it proceeds by the spinodal mechanism, which led to the formation of a homogeneous and dense array of submicron-sized Ge particles. The agglomeration of thicker Ge layers occurs non-uniformly over the surface and lead to the formation of particles, which differ in size and shape, with a bimodal distribution. An analysis of the shape of Ge particles shows that their large values of the contact angles and aspect ratios (height of particles divided by their lateral dimension) are the result of the excess of the Ge/SiO$_2$ interface energy over the SiO$_2$ surface energy. Our study determines the conditions of obtaining the surface coatings of submicron-sized dielectric Ge particles using the dewetting phenomenon depending on d_{Ge} and annealing temperature (T_{ann}).

Results

Behavior of 10–40 nm Ge layers on SiO$_2$ under annealing.

It was shown that low-temperature (up to 200 °C) Ge grown on SiO$_2$ forms polycrystalline Ge layers[40], which remain continuous and exhibit a high hole mobility after the annealing at temperatures up to 500 °C[41]. The annealing of our samples at 550 °C and lower temperatures does not lead to the formation of three-dimensional particles. The changes in the surface morphology are observed after the annealing at temperatures higher than 550 °C (Fig. 1). The changes occur through the appearance of undulations on the surface of Ge layers. This becomes visible in the SEM images[42] due to the difference in the atomic number between Ge from one side and, Si and oxygen from the other, at which the surface areas with thicker Ge layers on SiO$_2$ look brighter (Fig. 1d). In the case of the thinner (~20 nm) Ge layers, the distance between protuberances (Fig. 1a) is significantly smaller in comparison with that for the thicker Ge layers (Fig. 1b,c). Since the Ge layers are polycrystalline, their surface consists of areas with different crystalline orientations[41]. Although we do not know the size distribution of grains and their orientation with respect to the substrate surface, it is reasonable to assume that surface areas with grains with certain crystalline orientations may grow due to the Ge consumption from other areas. This may explain the appearance of protuberances on the surface at the relatively low annealing temperatures.
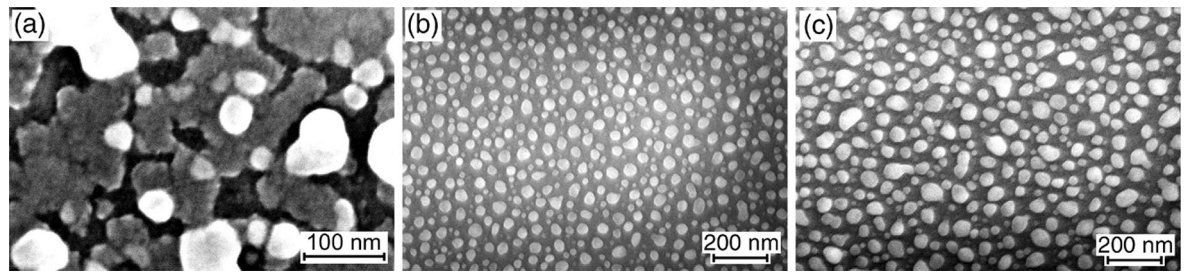
Figure 2. SEM images of Ge layers deposited on SiO_2 at RT with a subsequent annealing in vacuum after the exposure to the air: (**a**) 20 nm Ge layer annealed at 580 °C, (**b**) and (**c**) 10 and 20 nm Ge layers, respectively, annealed at 600 °C.
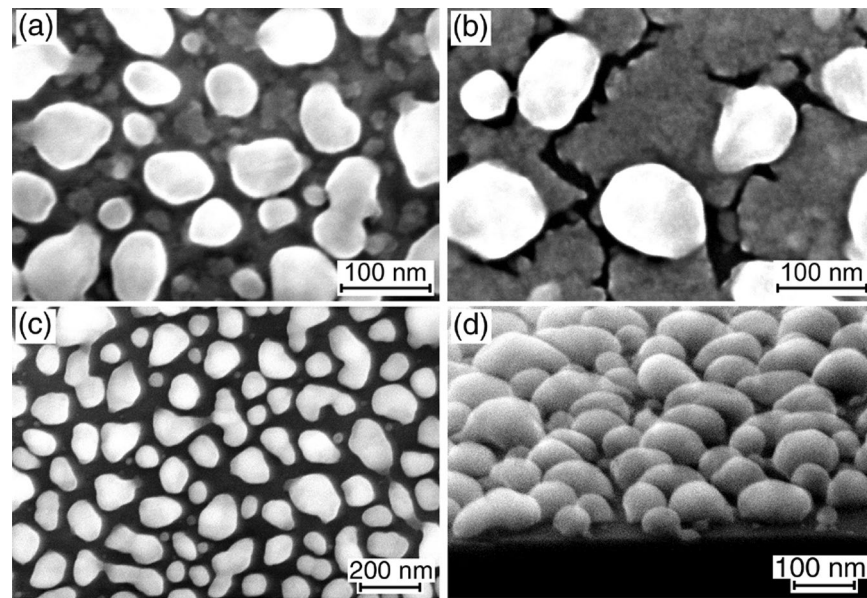

Figure 3. SEM images of the samples covered with (**a**) 30 and (**b**) 40 nm Ge layers after the annealing at 600 °C and (**c**) with the 40 nm Ge layer after the annealing at 800 °C. The image in (**d**) is taken at a glancing angle of about 10° for the sample with the 40 nm Ge layer after the annealing at 700 °C.

After the annealing at 580 °C for 30 min, the partial agglomeration of 10 and 20 nm Ge layers is observed. It consists in the formation of relatively large particles near holes shaped as narrow channels and small particles atop the remaining areas of the continuous Ge layer, as shown in Fig. 2a. Longer anneals (~ 2 h) at 580 °C do not lead to the complete disappearance of remaining areas of the Ge layers between the particles. The annealing at 600 °C ensures complete agglomeration of the Ge layers into compact particles (Fig. 2b). However, their average size is smaller than that of the particles after the annealing at 580 °C. This indicates that the particle formation mechanisms are different at the relatively low and high temperatures. The annealing at 800 °C, compared with the annealing at 600 °C, results in the formation of more compact particles with a more uniform shape, whereas their concentration and average size do not differ significantly.

The agglomeration of 30 and 40 nm Ge layers at 600 °C is partial (Fig. 3a,b). The dewetting proceeds through the development of large thickness perturbation of the Ge layers and the simultaneous formation of narrow channels (Fig. 3b). The ratio between these two processes also has a strong dependence on the annealing temperature. The remaining areas of the Ge layers between Ge particles completely disappear after the annealing of 30 and 40 nm Ge layers at 700 and 800 °C (Fig. 3c,d), respectively, and the particles acquires a compact shape with aspect ratios of about 0.5 (Fig. 3d). It can be noted that higher annealing temperatures are usually required to initiate the dewetting process in thicker layers of many materials[1,43], including Si on SiO_2[2,39].

The protuberances on the surface after the annealing at relatively low temperatures, the same as grains of the initial polycrystalline Ge layers, have a large scatter in size and random distribution over the surface[41]. Therefore, the subsequent appearance of channels in thinned areas of the Ge layers can be associated with grain boundaries. In contrast, after annealing at the high temperatures, the concentration of Ge particles is much higher than that of the protuberances, and they are uniformly distributed over the surface. This may indicate that their formation is not related to the location of grain boundaries. In addition, the Ge particle concentration gradually increases with the increasing d_{Ge}, while such dependence for the grain concentration has not observed[41].

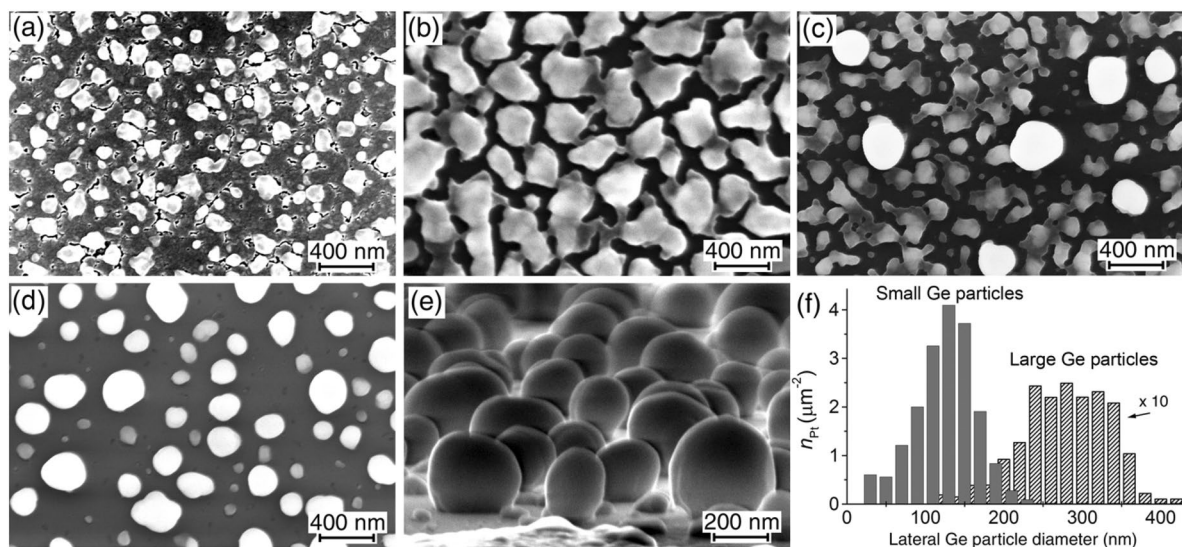**Figure 4.** SEM images of the samples with the 60 nm Ge layers after the annealing at (**a**) 650, (**b**) 700, (**c**) 800 and (**d**,**e**) 850 °C. Images (**a–d**) are taken at the normal electron beam incidence and (**c**) at the glancing angle of about 7° relative to the sample surface. (**f**) The bimodal distribution of Ge particles on SiO_2 as a function of their lateral diameter, which is obtained for the sample with the 60 nm Ge layer after its annealing at 800 °C.

Dewetting behavior of 60–86 nm Ge layers. The surface morphology of the samples with 60 and 70 nm Ge layers exhibits a strong dependence on T_{ann}, as shown in Fig. 4a–e. The annealing at 650 °C results in the surface morphology (Fig. 4a) similar to that observed for the 40 nm Ge layers after 600 °C. However, the annealing at 800 °C leads to a significantly different morphology. It consists in the formation of a bimodal distribution of Ge particles which are different in size and shape (Fig. 4c,f). This arises from the specific features of the Ge layer evolution under annealing. It begins from the formation of large Ge particles and areas of the thinned Ge layer between them. These areas then turn into groups of smaller Ge particles after the annealing at 850 °C (Fig. 4d). Some of the Ge particles acquire a shape close to spherical with the aspect ratio of about 1, as shown in Fig. 4e.

The longer annealing (~2 h) at temperatures up to 800 °C results only in slight surface morphology changes making the Ge particles more compact. This indicates that the main changes in the surface morphology at each temperature occur during the initial period of annealing time. Then, the rate of change decreases as the total energy of surface layers approaches its minimum. This suggests that the surface morphology can depend on the rate at which the annealing temperature is reached. However, in this study, only the rather high rate of 4 °C/s is used.

The break-up behavior of 86 nm Ge layers at the initial stage under the annealing is similar to that of thinner Ge layers. At 700 °C, this consists in the formation of Ge protrusions like three-dimensional particles only due to the thinning of the surrounding Ge layer (Figs. 1b, 5a), that is, without the appearance of holes shaped as channels. This may be interpreted as the Ge layer thickness undulation. As was mentioned for the initial stage of thin Ge layer transformation, the undulation formation can be associated with different crystalline orientations of Ge grains in the Ge layers, which may have different growth rates during annealing.

The break-up development at the high temperature of 800 °C occurs through the compact hole formation in the Ge layer (Fig. 5b). After the annealing at 850 °C, the formation of Ge particles with bimodal distributions in size and shape is observed (Fig. 5c,d), similar to the behavior of 60 and 70 nm Ge layers after the annealing at 800 °C. The compact particles of larger sizes are characterized by a large aspect ratio up to about 1.0 (Fig. 5d). It can be mentioned that the dewetting in Si on SiO_2 results in the formation of Si particles with significantly smaller aspect ratios up to 0.4[44,45].

The formation of holes, as well as channels during the annealing of thinner Ge layers is aimed at the exposing of SiO_2 surface areas. This occurs for the surface energy minimization, since the SiO_2 surface energy is much smaller than that of Ge.

Surface morphology after the annealing at 900 °C. The annealing of 40–86 nm Ge layers at 900 °C lead to the formation of compact Ge particles, the shape of which becomes more uniform (Fig. 6). As expected, a certain Ge amount is removed from the surface due to the annealing. This process was studied earlier[21,38,46] and consisted in the formation of volatile SiO and GeO molecules by the reaction

$$SiO_2 + Ge \rightarrow SiO \uparrow + GeO \uparrow, \tag{1}$$

occuring at the boundary between SiO_2 and Ge particles along their perimeter. This is confirmed by the fact that voids (pits) are formed in SiO_2 around relatively large Ge particles, and they also appears at the locations of small Ge particles after their complete removal (Fig. 6). The similar result was observed for SiGe-on-SiO_2 structures
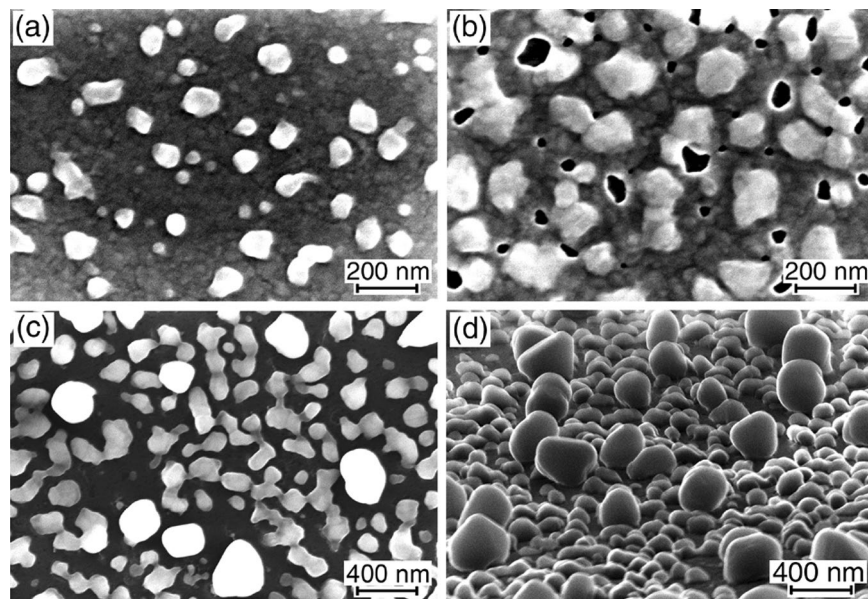
Figure 5. SEM images of the samples with 86 nm Ge layers on SiO$_2$ after the annealing at (**a**) 700, (**b**) 800 and (**c,d**) 850 °C. Images (**a**–**c**) are taken at the normal electron beam incidence and (d) at a glancing angle of about 10° relative to the sample surface.
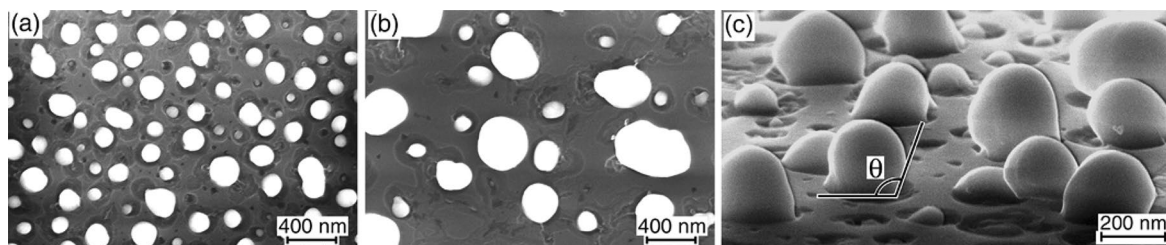

Figure 6. (**a**–**c**) SEM images of the samples with 40, 70 and 60 nm Ge layers on SiO$_2$ after the annealing at 900 °C for 30 min. Images (**a,b**) are taken at the normal electron beam incidence and (**c**) at a glancing angle of about 5° relative to the sample surface. The particle contact angle is shown in (**c**).

with strained SiGe layers after their high-temperature annealing at 880 °C[47]. The interaction of Si particles with SiO$_2$ was previously studied in detail[48–50], and it revealed the features similar to those observed in our case.

Discussion. A general picture of the Ge layer transformations caused by the dewetting from the SiO$_2$ surface is schematically shown in Fig. 7 in coordinates d_{Ge} and T_{ann}. The behavior of 10 nm Ge layers on SiO$_2$ under annealing was previously investigated by Wakayama et al.[29]. They observed the Ge particle formation at about 300 °C when it was carried out in a vacuum chamber without the sample exposition to the air. The significantly higher temperatures require for the Ge particle formation, in our case, can be associated with the presence of the native Ge oxide, which can interfere with the dewetting process[39]. The beginning of the Ge particle formation may indicate that the stabilizing effect of the native Ge oxide becomes insufficient at 580 °C. Probably, at this temperature, its partial decomposition occurs with the formation of volatile GeO molecules. This is consistent with the fact that the onset of the dewetting process is observed at about the same temperatures around 600 °C for the Ge layers in the wide range of d_{Ge} (Fig. 7a). The GeO$_2$ surface energy is less than that of SiO$_2$[51], and it is much smaller than the Ge surface energy. Therefore, the Ge layers covered with the native Ge oxide are thermally stable. Conditions for their agglomeration into particles appear when this Ge oxide begins to be desorbed with the formation of bare Ge surface areas. The similar effect of the native oxide could also manifest itself in the behaviour of thin crystalline Si layers on SiO$_2$, for which the Si particle formation was observed after the annealing at significantly higher temperatures (> 750 °C) for commercial silicon-on-insulator structures[39,52–54] than that ($T_{ann} = 550$ °C) for the bare amorphous Si layers on SiO$_2$[29].

One of the approaches to obtaining clean Ge surfaces consists in an ex situ wet etching/oxidation process which provides removal of metallic and carbon contaminations. This is followed by in situ thermal annealing in vacuum at 500–600 °C[55,56] or flash anneals at about 750 °C[57,58] to remove Ge oxide. In our case, the initial surface of deposited Ge layers does not contain impurities. Therefore, the onset of the dewetting process, which is observed at 600 °C, can be associated with the removal of native oxide from the Ge surface.
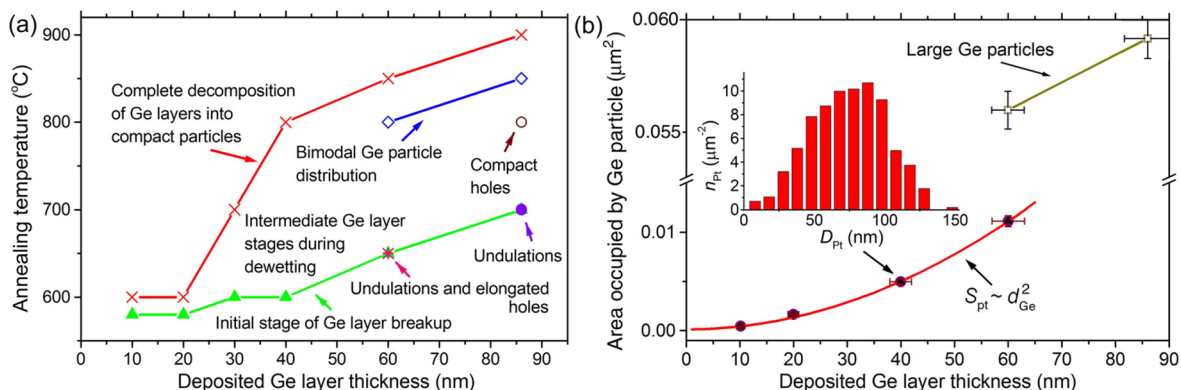
Figure 7. (**a**) Schematic diagram of Ge layer transformations on SiO$_2$ caused by dewetting, presented in coordinates d_{Ge} and T_{ann}. (**b**) Average surface area occupied by a Ge particle after the dewetting of Ge layers from SiO$_2$ as a function of d_{Ge}. The annealing of the deposited Ge layers is performed at 800 °C for 30 min for the layer thicknesses of 10, 20 40 and 60 nm, and at 850 °C for 86 nm. The concentration Ge particle distribution as a function of their lateral diameter, obtained after the dewetting of the 40 nm Ge layer, is shown in the inset.

The averaged lateral area (S_{pt}) occupied by a Ge particle increases proportionally to $\sim d_{Ge}^2$ (Fig. 7b). A typical concentration distribution (n_{pt}) of compact Ge particles as a function of their diameter is shown in the inset to Fig. 7b. The obtained relation $S_{pt} \sim d_{Ge}^2$ means that $D_{pt} \sim d_{Ge}$, where D_{pt} is the average particle diameter. A linear relation between D_{pt} and d_{Ge} is usually observed when metal particles are formed by dewetting[1,31]. Such a relation between D_{pt} and d_{Ge} corresponds to the decrease in the total particle concentration N_{pt} as a function of d_{Ge} as $N_{pt} \sim 1/d_{Ge}^2$ [43]. The strong decrease of N_{pt} as a function of increasing d_{Ge} also occurs during the Ge deposition on Si(100)[5].

There are two mechanisms of the dewetting phenomenon, which are usually distinguished in thin layers deposited on non-wettable surfaces. One of them is called spinodal dewetting, which is associated with a spontaneous amplification of layer thickness perturbation[6,59]. The spontaneous growth of the perturbation can eventually reach the substrate surface. Dewetting can also proceed through the hole formation, which begins at the inhomogeneities in the layer surface or layer/substrate interface[6,51]. In our case, as discussed below, the first or both dewetting mechanisms are involved, depending on d_{Ge} and T_{ann}.

At the relatively high temperatures the compact Ge particle formation is accompanied by the rupture of continuous Ge layers with the appearance of holes shaped as narrow 10–30 nm wide channels (Fig. 1b). The channel width is approximately equal to the distance between the Ge particles arising from the agglomeration of 10 and 20 nm Ge layers. This results in the narrow temperature range ($\sim$ 580 to 600 °C) from the initial agglomeration stage to the formation of compact Ge particles (Figs. 2, 7a). However, the channel width is smaller than the distance between Ge particles (protrusions) in the case of the thicker (30–60 nm) Ge layers. This lead to the intermediate presence of thinned areas of the Ge layers near the Ge protrusions and particles. The further thinning of the thinned areas makes them thermally unstable and causes their agglomeration into the groups of relatively small particles (Figs. 3, 4, 5).

The Ge particles form a dense array for which a short-range order in the Ge particle spatial distribution can be expected. To reveal this, we calculate the pair correlation function of the mass centers of Ge particles (Fig. 8). For the case of 10–60 nm Ge layers, the pair correlation functions exhibit well pronounced maxima (Fig. 8a) at the preferable particles spacing (λ_m). The presence of the maxima is the feature of the spinodal mechanism of the dewetting process[60,61]. The other feature of spinodal dewetting is the quadratic dependence of λ_m on the thickness of deposited layers[61–64]. In our case, such dependence looks as $\lambda_m(nm) \approx 44(nm) + 0.043(nm^{-1}) \times d_{Ge}^2$ (the inset in Fig. 8a). It shows that as $d_{Ge} \to 0$, L does not $\to 0$, as would be expected. This deviation from the typical behavior may indicate the influence of native Ge oxide residues on the layer thickness undulation at the initial dewetting stage. This may also reflect the influence of polycrystalline nature of the Ge layers, if the size of Ge grains does not tend to 0 with the decreasing Ge layer thickness.

Maxima are not observed in the pair correlation functions of large Ge particles which are formed using 60 and 86 nm Ge layers (Fig. 8b). The distance between them is so great that they do not influence each other. This indicates that the large Ge particle formation mechanism cannot be attributed to the spinodal one. This is despite the fact that the gradual change in the surface morphology is observed through the formation of protrusions without holes at the initial stage (Figs. 1b, 5a). As mentioned above, their formation can be associated with the surface areas of initial Ge grains with certain crystalline orientations.

In the case of liquid-state dewetting, the shape of droplets (particles) is characterized by the contact angle θ which is described by the Young's equation[1,65]. This can be written in the form:

$$\gamma_{is} = \gamma_{ss} - \gamma_{ps} \cos(\theta) \tag{2}$$

where γ_{is} is the particle/substrate interfacial tension; γ_{ss} and γ_{ps} are the surface tensions of the substrate and particles, respectively. It is important to note that Eq. (2) is valid for describing thermodynamically equilibrium particle shapes. In the case of solid-state dewetting, the particle shape is determined by kinetic factors, such as
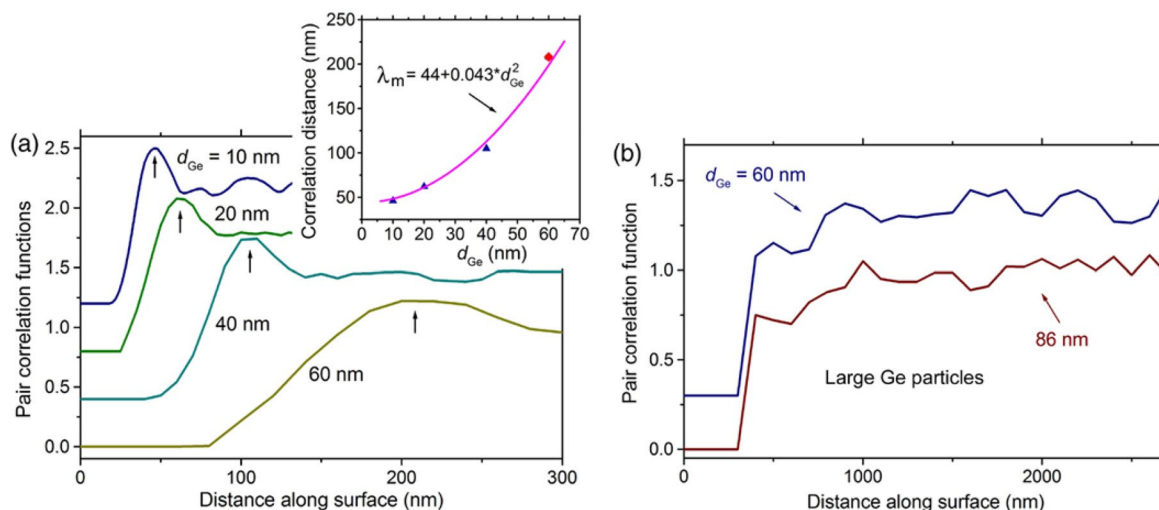
Figure 8. Pair correlation functions of the mass centers of the Ge particles on SiO$_2$ obtained after the dewetting of relatively (**a**) thin and (**b**) thick Ge layers. The Ge layer thicknesses are marked at the corresponding curves. The data for the 60 nm Ge layer in (**a**) are obtained without taking into account large Ge particles. The functions are offset from each other by 0.4 on (**a**) and by 0.6 on (**b**) for their separation. The pair correlation length (λ_m), which positions are marked in (**a**) by arrows, as a function of the deposited Ge layer thickness is shown in the inset.

nucleation of crystal particles with an arbitrary orientation relative to a substrate surface and growth rates which depend on the crystalline orientation of particle surface planes. This forms particles which can differ in shape. However, if the particle formation conditions are not far from equilibrium, their shape can be characterized by Eq. (2) using surface and interface energies instead of tensions[66,67]. In our case, some scatter of θ can be seen in Fig. 6c even when the high T_{ann} (900 °C) is used. This means that the particle formation conditions are not very close to equilibrium. Nevertheless, Eq. (2) can be used for the semi-quantitative estimates of the energy parameters of surface structures.

Assuming that the surface energies of amorphous SiO$_2$ and Ge are known, we can use Eq. (2) to determine the interface energy between the Ge particles and SiO$_2$ as a function of the contact angle. The surface energy of Ge ranges from 1.32 to 1.71 J/m^2, depending on the crystalline orientation of its surface[68,69]. γ_{fs} = 1.5 J/m^2 can be taken as an average value. The surface energy γ_{ss} of SiO$_2$ can be determined through the contact angles of droplets (particles), which are formed due to the dewetting of various liquids on SiO$_2$[70,71], including melted Ge[34]. This gives γ_{ss} ~ 0.05 J/m^2. The SiO$_2$ surface energy obtained by calculations and other experimental methods exhibits much larger values γ_{ss} ~ 0.4 J/m^2[72–74]. As was shown by Bangera and Appaiah[75], this is a typical relation between of the surface energy values when they are smaller by a factor of ~ 10 if they are determined in the liquid-state dewetting experiments. Just as it was done by Cheynis et al.[33] in their analysis of the solid-state dewetting, the larger values of γ_{ss}, namely ≈ 0.4 J/m^2, should be used in our estimations of γ_{is}. In Fig. 6c are the SEM images of Ge particles with θ ranges from about 90° to 120° which are formed even around one particle. Taking θ = 105° as an average value, the Eq. (2) gives γ_{is} ≈ 0.8 J/m^2. This value is consistent with the literature data, according to which the Ge/SiO$_2$ interface energy is larger than the SiO$_2$ surface energy[73,74]. In the structures with such relationships between γ_{is} and γ_{ss}, the size of the base of particles should be smaller than their lateral dimension. For comparison, in the structures of SiGe particles on Si surfaces, θ < 90° and, hence, the SiGe/Si γ_{is} of is smaller than the Si γ_{ss}[5]. This may indicate that a larger θ may be associated with a larger driving force for dewetting. This is consistent with the fact that the dewetting in Ge/SiO$_2$ is characterized by larger θ values and occurs at a lower temperature in comparison with Ge/Si which requires higher temperatures to intiate the dewetting and leads to smaller θ values[5]. It can be noted that there is an estimation of the driving force for the dewetting in Si on SiO$_2$ structures, which resulted in 14 eV/nm[22].

The surface morphology evolution due to dewetting can occur simultaneously over the entire surface. This was observed in the structures such as Ge/Si(111)[42,76] and Ge/SiO$_2$[29,33,34]. If the driving force for dewetting is relatively week and the surface morphology transformation begins from defects, the dewetting develops through a gradual propagation along the surface. Such behavior takes place in the structures of Ge/Si(100)[77–79] and Si(crystalline)/SiO$_2$[3,41,80–82]. The dewetting conditions may appear in the structure with the increasing elastic strain in it, as was observed when the thickness of Ge layers on Si(111) was increased at a given substrate temperature[83]. The surface layer energy calculations for the Ge/Si(100) structures showed that it has a gentle minimum as a function of the contact angle. This was proposed as an argument for explaining the large scatter of contact angles[5]. In our case of polycrystalline Ge layers up to 60 nm thick grown on SiO$_2$ at RT, the dewetting phenomenon occurred simultaneously over the entire surface with the formation of Ge particles in the shapes with a relatively small scatter of contact angles. This indicates a relatively large driving force for the dewetting in Ge/SiO$_2$ relative to Si/SiO$_2$.

Conclusion. The initiation of dewetting in the 10–86 nm Ge layers on SiO_2 after the exposure to the air begins at temperatures of 580–700 °C, depending on the layer thickness. At the relatively low temperatures, this occurs through the appearance of undulation on the surface of Ge layers, which can be associated with their polycrystalline structure containing grains with different crystalline orientations. Then, the formation of Ge particles is accompanied by a rupture of the Ge layers with the appearance of narrow channels or rounded holes in the Ge layers with the thicknesses of 10–60 and 86 nm, respectively. The distance between particles is comparable in magnitude with the channel widths in the 10–20 nm Ge layers. The formation of compact Ge particles in this case is completed at 600 °C. For the 30–86 nm Ge layers, the width of the channels or holes is less than the distance between the particles. As a result, along with them, the thinned Ge layer areas are formed at the intermediate break-up stage. As these areas are thinned further, they break up into smaller particles. This leads to the bimodal distribution of particles which differ both in size and in shape. Such features as the existence of a maximum in the particle pair correlation functions and the quadratic dependence of the corresponding particle spacing on d_{Ge}, may indicate the spinodal dewetting mechanism for the formation of small particles at the relatively high temperatures. The larger particles, which begin to form first, acquire a high aspect ratio up to about 1.0. The contact angles of the Ge particles are larger than 90°, thus, indicating that the interface energy between the Ge particle and SiO_2 is greater than the SiO_2 surface energy.

Methods

Sample preparation. The Si(100) plates covered with a 1 μm thick thermal SiO_2 film are used as substrates, the same as in[34]. The Ge deposition is carried out in an ultrahigh-vacuum chamber, with a base pressure of about 1×10^{-10} Torr, which was manufactured by Omicron. A Knudsen cell with a BN crucible is used for the Ge deposition at a rate of ~ 1.0 nm/min. The Ge deposition rate was calibrated as a function of Knudsen cell temperature by means of measuring submonolayer Ge coverages on Si(111) with scanning tunneling microscopy[84]. The accuracy of setting the Ge layer thickness is determined by the accuracy of measuring the Ge deposition rate, which is within 5%. After the substrate degassing by heating in the growth chamber at about 450 °C, the Ge deposition is performed without substrate annealing. During the Ge deposition the substrate temperature may gradually increase from RT due to the radiation from the Knudsen cell. The substrates covered with Ge layers from 10 to 86 nm thick are cut into samples, which are then annealed in the vacuum conditions of a MILA-5000 furnace with a residual pressure of ~ 1×10^{-7} Torr at various temperatures up to 900 °C for 30 or 120 min. The heating and cooling temperature rates are about 4 and 15 °C/s, respectively.

Material characterization. The sample surface morphology is studied using a Pioneer scanning electron microscope (SEM) manufactured by Raith. The sample surface observation is performed at different electron beam incident angles, including obtaining the images of sample cross-sections, similar to that used elsewhere[34]. All SEM images presented here were taken from the samples after their annealing for 30 min. The average value of areas occupied by a Ge particle is obtained from SEM images using Gwyddion software. The spread of this value between surface areas is less than 5%.

References

1. CV Thompson 2012 Solid-state dewetting of thin films Annu. Rev. Mater. Res. 42 399 434
2. F Cheynis E Bussmann F Leroy T Passanante P Müller 2012 Stress effects on solid-state dewetting of nano-thin films Int. J. Nanotechnol. 9 396 411
3. F Leroy Ł Borowik F Cheynis Y Almadori S Curiotto M Trautmann JC Barbé P Müller 2016 How to control solid state dewetting: A short review Surf. Sci. Rep. 71 391 409
4. AA Shklyaev AE Budazhapova 2016 Ge deposition on Si(100) in the conditions close to dynamic equilibrium between islands growth and their decay Appl. Surf. Sci. 360 1023 1029
5. AA Shklyaev AE Budazhapova 2017 Submicron- and micron-sized SiGe island formation on Si(100) by dewetting Thin Solid Films 642 345 351
6. J Ye D Zuev S Makarov 2019 Dewetting mechanisms and their exploitation for the large-scale fabrication of advanced nanophotonic systems Int. Mater. Rev. 64 439 477
7. F Ruffino MG Grimaldi 2015 Controlled dewetting as fabrication and patterning strategy for metal nanostructures Phys. Status Solidi (a) 212 1662 1684
8. T Chung Y Lee MS Ahn W Lee SI Bae CSH Hwang KH Jeong 2019 Nanoislands as plasmonic materials Nanoscale 11 8651 8664
9. M Rahaman AG Milekhin A Mukherjee EE Rodyakina AV Latyshev VM Dzhagan DRT Zahn 2019 The role of a plasmonic substrate on the enhancement and spatial resolution of tip-enhanced raman scattering Faraday Discuss. 214 309 323
10. AI Kuznetsov AE Miroshnichenko ML Brongersma YS Kivshar Luk'yanchuk B 2016 Optically resonant dielectric nanostructures Science 354 2472
11. H Kallel A Arbouet G BenAssayag A Chehaidar A Potié B Salem T Baron V Paillard 2012 Tunable enhancement of light absorption and scattering in $Si_{1-x}Ge_x$ nanowires Phys. Rev. B 86 085318
12. X Zhu W Yan U Levy NA Mortensen A Kristensen 2017 Resonant laser printing of structural colors on high-index dielectric metasurfaces Sci. Adv. 3 e1602487
13. DG Baranov DA Zuev SI Lepeshov OV Kotov AE Krasnov AB Evlyukhin BN Chichkov 2017 All-dielectric nanophotonics: The quest for better materials and fabrication techniques Optica 4 814 825
14. V Poborchii A Shklyaev L Bolotov N Uchida T Tada ZN Utegulov 2017 Photonic metasurface made of array of lens-like SiGe Mie resonators formed on (100) Si substrate via dewetting Appl. Phys. Express 10 125501
15. J Tian H Luo Q Li X Pei K Du M Qiu 2018 Near-infrared super-absorbing all-dielectric metasurface based on single-layer germanium nanostructures Laser Photon. Rev. 12 1800076

16. M Bouabdellaoui S Checcucci T Wood M Naffouti RP Sena K Liu CM Ruiz D Duche J Rouzo le L Escoubas G Berginc N Bonod M Zazoui L Favre L Metayer A Ronda I Berbezier D Grosso M Gurioli M Abbarchi 2018 Self-assembled anti-reflection coatings for light trapping based on SiGe random metasurfaces Phys. Rev. Mat. 2 035203

17. K Li J Li C Reardon CS Schuster Y Wang GJ Triggs N Damnik J Müenchenberger X Wang ER Martins TF Krauss 2016 High speed e-beam writing for large area photonic nanostructures—a choice of parameters Sci. Rep. 6 32945

18. WK Lee S Yu CJ Engel T Reese D Rhee W Chen TW Odom 2017 Concurrent design of quasi-random photonic nanostructures Proc. Natl. Acad. Sci. USA 114 8734 8730

19. S Yu C Wang Y Zhang B Dong Z Jiang X Chen W Chen C Sun 2017 Design of non-deterministic quasi-random nanophotonic structures using Fourier space representations Sci. Rep. 7 3752

20. M Dupré L Hsu B Kanté 2018 On the design of random metasurface based devices Sci. Rep. 8 7162

21. AA Shklyaev M Shibata M Ichikawa 2000 High-density ultrasmall epitaxial Ge islands on Si(111) surfaces with a SiO_2 coverage Phys. Rev. B 62 1540 1543

22. A Barski M Derivaz JL Rouviиre D Buttard 2000 Epitaxial growth of germanium dots on Si(001) surface covered by a very thin silicon oxide layer Appl. Phys. Lett. 77 3541 2543

23. AA Shklyaev M Ichikawa 2002 Effect of interfaces on quantum confinement in Ge dots grown on Si surfaces with a SiO_2 coverage Surf. Sci. 514 19 26

24. I Berbezier A Karmous A Ronda A Sgarlata A Balzarotti P Castrucci M Scarselli M Crescenzi De 2006 Growth of ultrahigh-density quantum-confined germanium dots on SiO_2 thin films Appl. Phys. Lett. 89 063122

25. CD Poweleit CW Hu IS Tsong J Tolle J Kouvetakis 2007 Optical characterization of $Si_{1-x}Ge_x$ nanodots grown on Si substrates via ultrathin SiO_2 buffer layers J. Appl. Phys. 101 114312

26. M Aouassa I Berbezier L Favre A Ronda M Bollani R Sordan A Delobbe P Sudraud 2012 Design of free patterns of nanocrystals with ad hoc features via templated dewetting Appl. Phys. Lett. 101 013117

27. KA Lozovoy AP Kokhanenko VV Dirko NYu Akimenko AV Voitsekhovskii 2019 Evolution of epitaxial quantum dots formed by Volmer–Weber growth mechanism Cryst. Growth Des. 19 7015 7021

28. KA Lozovoy AG Korotaev AP Kokhanenko VV Dirko AV Voitsekhovskii 2020 Kinetics of epitaxial formation of nanostructures by Frank–van der Merwe, Volmer–Weber and Stranski–Krastanow growth modes Surf. Coat. Technol. 384 125289

29. Y Wakayama T Tagami S Tanaka 1999 Three-dimensional islands of Si and Ge formed on SiO_2 through crystallization and agglomeration from amorphous thin films Thin Solid Films 350 300 307

30. E Sutter P Sutter 2006 Assembly of Ge nanocrystals on SiO_2 via a stress-induced dewetting process Nanotechnology 17 3724 3727

31. Y Kojima T Kato 2008 Nanoparticle formation in Au thin films by electron-beam-induced dewetting Nanotechnology 19 255605

32. HJ Choe SH Kwon C Choe JJ Lee CH Woo 2016 Sn microparticles made by plasma-induced dewetting Thin Solid Films 620 165 169

33. F Cheynis F Leroy T Passantante P Müller 2013 Agglomeration dynamics of germanium islands on a silicon oxide substrate: A grazing incidence small-angle X-ray scattering study Appl. Phys. Lett. 102 161603

34. C Dabard AA Shklyaev VA Armbrister AL Aseev 2020 Effect of deposition conditions on the thermal stability of Ge layers on SiO_2 and their dewetting behavior Thin Solid Films 693 137681

35. AA Shklyaev SP Cho Y Nakamura N Tanaka M Ichikawa 2007 Influence of growth and annealing conditions on photoluminescence of Ge/Si layers grown on oxidized Si surfaces J. Phys. Condens. Matter 19 136004

36. AA Shklyaev KN Romanyuk SS Kosolobov 2014 Surface morphology of Ge layers epitaxially grown on bare and oxidized Si(001) and Si(111) substrates Surf. Sci. 625 50 56

37. Y Nakamura M Ichikawa 2015 Formation of epitaxial nanodots on Si substrates with controlled interfaces and their application Jpn. J. Appl. Phys. 54 07JD01

38. AA Shklyaev M Shibata M Ichikawa 1998 Nanometer-scale germanium islands on Si(111) surface windows formed in an ultrathin silicon dioxide film Appl. Phys. Lett. 72 320 322

39. M Trautmann F Cheynis F Leroy S Curiotto P Muller 2017 Interplay between deoxidation and dewetting for ultrathin SOI films Appl. Phys. Lett. 110 161601

40. K Toko R Yoshimine K Moto T Suemasu 2017 High-hole mobility polycrystalline Ge on an insulator formed by controlling precursor atomic density for solid-phase crystallization Sci. Rep. 7 16981

41. R Yoshimine K Moto T Suemasu K Toko 2018 Advanced solid-phase crystallization for high-hole mobility (450 cm^2 V^{-1} s^{-1}) Ge thin film on insulator Appl. Phys. Express 11 031302

42. A Shklyaev L Bolotov V Poborchii T Tada 2015 Properties of three-dimensional structures prepared by Ge dewetting from Si(111) at high temperatures J. Appl. Phys. 117 205303

43. PR Gadkari AP Warren RM Todi RV Petrova KR Coffey 2005 Comparison of the agglomeration behavior of thin metallic films on SiO_2 J. Vac. Sci. Technol. A 23 1152 1161

44. AA Shklyaev M Ichikawa 2002 Three-dimensional Si islands on Si(001) surfaces Phys. Rev. B 65 045307

45. M Naffouti T David A Benkouider L Favre A Ronda I Berbezier S Bidault N Bonod M Abbarchi 2016 Fabrication of poly-crystalline Si-based Mie resonators via amorphous Si on SiO_2 dewetting Nanoscale 8 2844 2849

46. S Fujita S Maruno H Watanabe M Ichikawa 1997 Nanofabrication using selective thermal desorption of SiO_2/Si induced by electron beams J. Vac. Sci. Technol. A 15 1493

47. Y Almadori L Borowik N Chevalier W Hourani F Glowacki JC Barbe 2016 From solid-state dewetting of ultrathin cSGOI films to $Si_{1-x}Ge_x$ nanocrystals stoïchiometry mastering J. Phys. Chem. C 120 7412 7420

48. K Sudoh M Naito 2010 Interfacial reaction of Si islands on SiO_2 during high-temperature annealing J. Appl. Phys. 108 083520

49. F Leroy Y Saito F Cheynis E Bussmann O Pierre-Louis P Müller 2014 Nonequilibrium diffusion of reactive solid islands Phys. Rev. B 89 235406

50. F Leroy Y Saito S Curiotto F Cheynis O Pierre-Louis P Müller 2015 Shape transition in nano-pits after solid-phase etching of SiO_2 by Si islands Appl. Phys. Lett. 106 191601

51. LPH Jeurgens Z Wang EJ Mittemeijer 2009 Thermodynamics of reactions and phase transformations at interfaces and surfaces Int. J. Mater. Res. 100 1281 1307

52. Y Ono M Nagase M Tabe Y Takahashi 1995 Thermal agglomeration of thin single crystal Si on SiO_2 in vacuum Jpn. J. Appl. Phys. Part 1 34 1728 1735

53. R Nuryadi Y Ishikawa M Tabe 2000 Formation and ordering of self-assembled Si islands by ultrahigh vacuum annealing of ultrathin bonded silicon-on-insulator structure Appl. Surf. Sci. 159–160 121 126

54. F Leroy F Cheynis T Passanante P Müller 2013 Influence of facets on solid state dewetting mechanisms: Comparison between Ge and Si on SiO_2 Phys. Rev. B 88 035306

55. K Prabhakarana T Ogino R Hull JC Bean LJ Peticolas 1994 An efficient method for cleaning Ge (100) surface Surf. Sci. 316 L1031 L1033

56. C Blumenstein S Meyer A Ruff B Schmid J Schäfer R Claessen 2011 High purity chemical etching and thermal passivation process for Ge (001) as nanostructure template J. Chem. Phys. 135 064201

57. JS Hovis RJ Hamers CM Greenlief 1999 Preparation of clean and atomically flat germanium (001) surfaces Surf. Sci. 440 L815 L819

58. WM Klesse G Scappucci G Capellini MY Simmons 2011 Preparation of the Ge (001) surface towards fabrication of atomic-scale germanium devices Nanotechnology 22 145604
59. FB Wyart J Daillant 1990 Drying of solids wetted by thin liquid films Can. J. Phys. 68 1084 1088
60. U Thiele M Mertig W Pompe 1998 Dewetting of an evaporating thin liquid film: Heterogeneous nucleation and surface instability Phys. Rev. Lett. 80 2869 2872
61. R Xie A Karim JF Douglas CC Han RA Weiss 1998 Spinodal dewetting of thin polymer films Phys. Rev. Lett. 81 1251 1254
62. J Bischof D Scherer S Herminghaus P Leiderer 1996 Dewetting modes of thin metallic films: Nucleation of holes and spinodal dewetting Phys. Rev. Lett. 77 1536
63. C Favazza R Kalyanaraman R Sureshkumar 2006 Robust nanopatterning by laser-induced dewetting of metal nanofilms Nanotechnology 17 4229 4234
64. H Krishna C Favazza AK Gangopadhyay R Kalyanaraman 2008 Functional nanostructures through nanosecond laser dewetting of thin metal films JOM 60 37 42
65. F Spaepen 1996 Substrate curvature resulting from capillary forces of a liquid drop J. Mech. Phys. Solids 44 675 681
66. G Whyman E Bormashenko T Stein 2008 The rigorous derivation of Young, Cassie Baxter and Wenzel equations and the analysis of the contact angle hysteresis phenomenon Chem. Phys. Lett. 450 355 359
67. L Makkonen 2016 Young's equation revisited J. Phys. 28 135001
68. AA Stekolnikov F Bechstedt 2005 Shape of free and constrained group-IV crystallites: Influence of surface energies Phys. Rev. B 72 125326
69. R Zhachuk S Teys J Coutinho 2013 Strain-induced structure transformations on Si(111) and Ge(111) surfaces: A combined density-functional and scanning tunneling microscopy study J. Chem. Phys. 138 224702
70. SR Narayan JM Day HL Thinakaran N Herbots ME Bertram CE Cornejo TC Diaz KL Kavanagh RJ Culbertson FJ Ark S Ram MW Mangus R Islam 2018 Comparative study of surface energies of native oxides of Si(100) and Si(111) via three liquid contact angle analysis MRS Adv. 3 3379 3390
71. B Baker N Herbots SD Whaley M Sahal J Kintz A Yano S Narayan AL Brimhall W-L Lee Y Akabane RJ Culbertson 2019 Surface energy engineering for LiTaO$_3$ and α-quartz SiO$_2$ for low temperature (< 220 °C) wafer bonding J. Vac. Sci. Technol. A 37 041101
72. J Mizele JL Dandurand J Schott 1985 Determination of the surface energy of amorphous silica from solubility measurements in micropores Surf. Sci. 162 830 837
73. J Du P Kroll 2010 Electronic structure and interfacial properties of Ge nanoclusters embedded in amorphous silica J. Non-Cryst. Solids 356 2448 2453
74. CY Chuang Q Li D Leonhardt SM Han T Sinno 2013 Atomistic analysis of Ge on amorphous SiO$_2$ using an empirical interatomic potential Surf. Sci. 609 221 229
75. AE Bangera K Appaiah 2019 A conditional justification for the determination of surface energy of solids using contact angle methods Mater. Chem. Phys. 234 168 171
76. AA Shklyaev KE Ponomarev 2015 Strain-induced Ge segregation on Si at high temperatures J. Cryst. Growth 413 94 99
77. PP Zhang B Yang PP Rugheimer MM Roberts DE Savage F Liu MF Lagally 2009 Influence of germanium on thermal dewetting and agglomeration of the silicon template layer in thin silicon-on-insulator J. Phys. D Appl. Phys. 42 175309
78. AA Shklyaev AV Latyshev 2016 Surface morphology transformation under high-temperature annealing of Ge layers deposited on Si(100) Nanosc. Res. Lett. 11 366
79. AA Shklyaev VA Volodin M Stoffel H Rinnert M Vergnat 2018 Raman and photoluminescence spectroscopy of SiGe layer evolution on Si(100) induced by dewetting J. Appl. Phys. 123 015304
80. F Cheynis E Bussmann F Leroy T Passanante P Müller 2011 Dewetting dynamics of silicon-on-insulator thin films Phys. Rev. B 84 245439
81. B Legrand V Agache JP Nys V Senez D Stievenard 2000 Formation of silicon islands on a silicon on insulator substrate upon thermal annealing Appl. Rev. Lett. 76 3271 3273
82. M Abbarchi M Naffouti B Vial A Benkouider L Lermusiaux L Favre A Ronda S Bidault I Berbezier N Bonod 2014 Wafer scale formation of monocrystalline silicon-based mie resonators *via* silicon-on-insulator dewetting ACS Nano 8 11181
83. AA Shklyaev AV Latyshev 2019 Electromigration effect on the surface morphology during the Ge deposition on Si(111) at high temperatures Appl. Surf. Sci. 465 10 14
84. AA Shklyaev AE Budazhapova 2017 Critical conditions for SiGe island formation during Ge deposition on Si(100) at high temperatures Mater. Sci. Semicond. Proc. 57 18 23

Acknowledgements

Author contributions

A.A.S. conceived and conducted the experiments. Both authors discussed the results, analyzed the data, and wrote the manuscript.

Competing interests

The authors declare no competing interests.

Additional information

Correspondence and requests for materials should be addressed to A.A.S.

Reprints and permissions information is available at www.nature.com/reprints.

Publisher's note Springer Nature remains neutral with regard to jurisdictional claims in published maps and institutional affiliations.